

Cite this: *J. Mater. Chem. B*, 2018,
6, 3894

A multifunctional luminogen with aggregation-induced emission characteristics for selective imaging and photodynamic killing of both cancer cells and Gram-positive bacteria†

Miaomiao Kang,[‡] Ryan T. K. Kwok,[‡] Jianguo Wang,[‡] Han Zhang,^d
Jacky W. Y. Lam,^{bd} Ying Li,^b Pengfei Zhang,^{ib} Hang Zou,^b Xingguo Gu,^{*be}
Feng Li^{*ac} and Ben Zhong Tang^{ib} ^{*bd}

The increasing impact of bacteria on cancer progression and treatments has been witnessed in recent years. Insufficient attention to cancer-related bacteria may lead to distant metastasis, poor therapeutic efficiency and low survival rates for cancers. Exploiting new approaches that enable selective imaging and effective killing of cancer cells and bacteria are thus of great value for the battle against cancers. Herein, we report an aggregation-induced emission (AIE) luminogen, namely **TPPCN**, with intense emission and efficient reactive oxygen species production for fluorescence imaging and killing cancer cells and Gram-positive bacteria. This work not only demonstrates the potential of AIE luminogens in comprehensive cancer treatments but also stimulates the enthusiasm of scientists to design more multifunctional AIE systems for both cancer and bacteria theranostics.

Received 2nd March 2018,
Accepted 11th May 2018

DOI: 10.1039/c8tb00572a

rsc.li/materials-b

Introduction

Health is one of the major concerns of people all over the world. As a fatal enemy, cancers continue to threaten humans and ultimately lead to death.¹ In recent years, general approaches including surgery, radiation, chemotherapy, and photodynamic therapy (PDT) have been widely used for cancer treatments.² However, these methods have undesirable side effects on the healthy tissues and belated efficient intervention to the malignant

tumor due to the lack of precise diagnosis and targeted therapy.³ Furthermore, more and more research findings suggest that cancer-associated bacteria seriously reduce the efficiency of cancer treatments.^{4,5} For example, some bacteria in the tumor microenvironment can enhance chemo-resistance through metabolizing chemotherapeutic drugs⁶ and modulating the autophagy of cancer cells.⁷ Certain Gram-positive bacteria, such as *Fusobacterium*, can promote cancer growth and metastasis by travelling with primary tumor cells to distant sites.⁸ Besides, surgical-site infection (SSI) mainly caused by the Gram-positive bacteria *Staphylococcus* and *Streptococcus* could also seriously weaken the prognosis of cancer.⁹ Thus, it is more desirable to develop antimicrobial agents for a more comprehensive therapeutic effect and higher survival rates in cancer treatments. Given the intimate affinity between bacteria and cancers, it should be of great clinical significance if we can develop an approach that enables the precise diagnosis and efficient therapy of cancer as well as effective identification and killing of pathogenic bacteria simultaneously.

The concept of theranostics that combines diagnostic imaging and therapeutic intervention in one pharmaceutical agent was proposed in 2002 and widely applied in the treatment of cancer and bacteria-related diseases.¹⁰ X-ray, ultrasound (US), photoacoustic imaging (PA), computed tomography (CT), magnetic resonance imaging (MRI) and positron emission tomography (PET) are the commonly used diagnostic techniques; however, they are relatively expensive and limited in real-time bacteria detection

^a Guangdong Provincial Key Laboratory of Brain Function and Disease, Zhongshan School of Medicine, Sun Yat-sen University, Guangzhou 510080, China. E-mail: lifeng@mail.sysu.edu.cn

^b Department of Chemistry, Hong Kong Branch of Chinese National Engineering Research Center for Tissue Restoration and Reconstruction, Institute of Advanced Study and Division of Life Science, The Hong Kong University of Science and Technology, Clear Water Bay, Kowloon, Hong Kong, China. E-mail: tangbenz@ust.hk

^c Department of Neurobiology and Anatomy, Zhongshan School of Medicine, Sun Yat-sen University, Guangzhou 510080, China

^d NSFC Center for Luminescence from Molecular Aggregates, SCUT-HKUST Joint Research Laboratory, State Key Laboratory of Luminescent Materials and Devices, South China University of Technology, Guangzhou, 510640, China

^e Beijing Advanced Innovation Center for Soft Matter Science and Engineering, Beijing University of Chemical Technology, Beijing 100029, China. E-mail: guxingguo@mail.buct.edu.cn

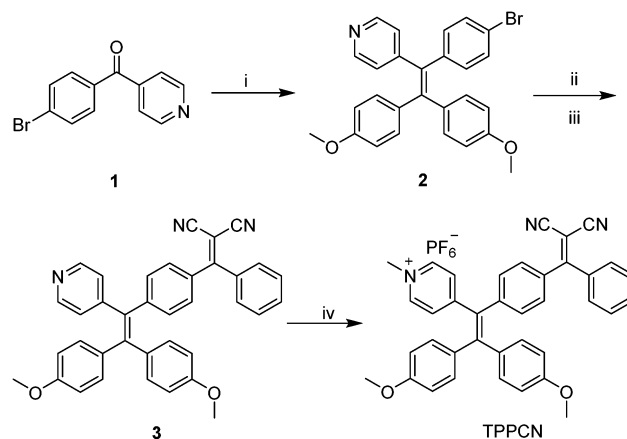
† Electronic supplementary information (ESI) available: Characterization of **TPPCN** and its intermediate; biocompatibility, ROS generation, staining and killing effect on U87 cells, and SEM studies of **TPPCN**. See DOI: 10.1039/c8tb00572a

‡ M. Kang and R. T. K. Kwok contributed equally to this work.

and tumor observation in intraoperative surgeries.¹¹ On the other hand, the classification of bacteria relies on the techniques of the Gram staining method, gene sequence identification and surface-enhanced Raman spectroscopy (SERS), which require either tedious labour or sophisticated equipment.¹² Furthermore, therapeutic agents must be additionally integrated through a complicated design for cancer treatment.^{10b,13} Therefore, developing a new strategy based on a single component will largely simplify the design procedure of the dual targeted theranostic system for both cancer and bacteria imaging and killing.

Fluorescent photosensitizers have attracted more and more attention in cancer imaging and therapy owing to their intrinsic advantages of superb sensitivity, good accessibility, low cost, reliable safety, and efficient reactive oxygen species (ROS) production.¹⁴ Conventional fluorophores often suffer from a notorious aggregation-caused quenching (ACQ) effect.¹⁵ This has left researchers with no choice but to study and utilize fluorophores as isolated molecules in very dilute solutions. However, the use of dilute solutions leads to serious photobleaching for imaging and less ROS production for PDT. Such attributes seriously impede the application of fluorophores in cancer cell imaging and therapy.¹⁶ Recently, our group observed a phenomenon of aggregation-induced emission (AIE), which is exactly the opposite of ACQ.¹⁷ Luminogens with the AIE characteristic (AIEgens) emit weakly or are non-emissive in solution but emit strongly in the aggregated state due to the restriction of intramolecular motions (RIMs). The AIE feature endows AIEgens with the intrinsic ability to resist the limitations of concentration and photobleaching.¹⁸ Moreover, some reported AIEgens demonstrated a unique aggregation-induced enhancement of ROS production, which enables them to be effective in PDT.¹⁹ For instance, TPE-IQ-2O, as the first AIEgen tested for its potential in cancer theranostics, was reported to possess the capacity of selective imaging and efficient PDT of cancer cells over normal ones, because the higher mitochondrial membrane potential (MMP) of cancer cells makes the positively charged TPE-IQ-2O more likely to specifically localize on the mitochondria of cancer cells by electrostatic interactions.²⁰ With respect to bacteria, many AIEgens have also been developed for detecting bacteria, differentiating dead or live bacteria, and killing pathogenic bacteria.²¹ The identification and killing of Gram-positive bacteria over Gram-negative ones, however, has rarely been reported by AIEgens.²² Therefore, it would be fascinating to develop multifunctional AIEgens for selective imaging and efficient killing of both cancer cells and Gram-positive bacteria.

In this contribution, we designed and synthesized a novel positively charged AIEgen, namely **TPPCN** (Scheme 1), with intense emission and high ROS production in the aggregated state. Like TPE-IQ-2O, **TPPCN** could fluorescently differentiate cancer cells from normal ones as a result of the electrostatic interaction and the MMP difference. **TPPCN** was also capable of distinguishing Gram-positive bacteria from Gram-negative ones, possibly due to the structural differences of Gram-positive and Gram-negative bacteria.²³ In addition, **TPPCN** aggregates could efficiently generate ROS under white light irradiation and cause damage to cancer cells and Gram-positive bacteria. To the best of



Scheme 1 The synthetic route to **TPPCN**. (i) 4,4'-Dimethoxyphenylmethanone, Zn, TiCl₄, THF, reflux, 5 h; (ii) *n*-BuLi, THF, *N,N*-dimethylbenzamide; (iii) TiCl₄, pyridine, malononitrile; (iv) CH₃I, toluene, reflux, overnight; KPF₆, acetone, r.t., 2 h.

our knowledge, this study represents the first example of a positively charged AIEgen as a dual targeted multifunctional agent for imaging and killing of both cancer and bacteria. It will stir up the enthusiasm of scientists to design more theranostic AIEgens for both cancer and pathogenic bacteria in the comprehensive treatment of cancers.

Results and discussion

Molecular design and photophysical properties

First, compound **1** was synthesized according to the literature²⁴ and then it was successfully converted to compound **2** by reaction with 4,4'-dimethoxyphenylmethanone through McMurry coupling in a moderate yield of 30%. Lithiation of compound **2** with *n*-BuLi at -78 °C and subsequent treatment with *N,N*-dimethylbenzamide resulted in the formation of a raw ketone compound, which then reacted with malononitrile to produce compound **3** under the catalysis of TiCl₄. Finally, the targeted **TPPCN** was obtained after methylation of compound **3** under refluxing in a high yield of 95%. The whole synthetic route is summarized in Scheme 1. All the structures of the synthetic compounds described here were confirmed by NMR and high-resolution mass spectroscopy (HRMS) (see the ESI,† Fig. S1–S9).

TPPCN in dichloromethane (DCM) exhibited an absorption maximum at 440 nm (Fig. 1A), which is located in the visible light range, causing less photodamage to living cells as compared to UV excitation. The photoluminescence (PL) spectra of **TPPCN** were then recorded carefully in hexane/DCM mixtures upon changing the composition of hexane (Fig. 1B).

TPPCN emitted faintly in hexane/DCM mixtures even when the hexane fraction (f_{Hexane}) reached 70%. When continuously increasing f_{Hexane} over 70%, fluorescence emerged gradually with a peak at 606 nm. The PL intensity at the f_{Hexane} of 90% was about 217 times higher than that in pure DCM solution. Bright yellow emission was also observed by the naked eye under a 365 nm UV lamp. Such strong emission is ascribed to

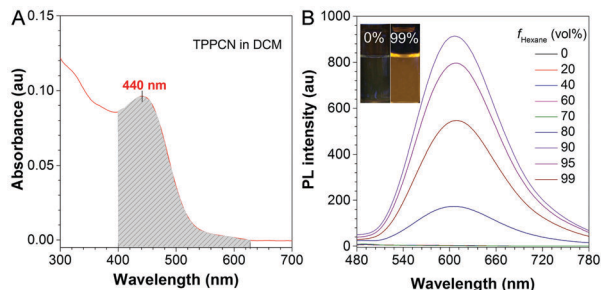


Fig. 1 (A) Absorption spectrum of **TPPCN** in dichloromethane (DCM). (B) Photoluminescence spectra of **TPPCN** in hexane/DCM mixtures with different fractions (f_{Hexane} , vol%); insets: photographs of **TPPCN** in hexane/DCM mixtures at f_{Hexane} of 0% and 99% taken under a 365 nm UV lamp. Concentration: 10 μM ; λ_{ex} : 440 nm.

the formation of aggregates upon increasing the fraction of the poor solvent hexane, which is indicative of a typical AIE characteristic for **TPPCN**. Notably, the PL intensity decreased slightly when the f_{Hexane} increased from 90% to 99%, which is possibly due to the precipitates of **TPPCN** on the wall of the cuvette. We further checked the absolute quantum yields of **TPPCN** in solution and aggregated states using a calibrated integrating sphere (Labsphere). The quantum yields (QYs) increasing from an undetectable value to 15.2% upon aggregate formation also demonstrated the AIE feature of **TPPCN**.

Mitochondrion-targeting ability of **TPPCN**

Before cell imaging, the cytotoxicity of **TPPCN** towards HeLa cells was first evaluated by using 3-(4,5-dimethyl-2-thiazolyl)-2,5-diphenyltetrazolium bromide (MTT) assay. MTT results suggested that the cell viability was negligibly affected even when the concentration of **TPPCN** reached 10 μM (see the ESI,† Fig. S10), indicating that the **TPPCN** exhibits low cytotoxicity and good biocompatibility to HeLa cells in this concentration range. Since **TPPCN** can form aggregates in aqueous solution (see the ESI,† Fig. S11), we applied **TPPCN** aggregates to stain the HeLa cells. As shown in Fig. 2A, the profile of the mitochondria was clearly observed with a bright blue-green colour, which comes from the fluorescence of **TPPCN**. Apparently, this reveals that **TPPCN** can selectively accumulate in the mitochondria and emit strong blue-green fluorescence. The specificity to mitochondria was also verified by co-staining **TPPCN** with a commercially available mitochondria imaging agent, MitoTracker Red FM (MTR). The blue-green emission from **TPPCN** was greatly consistent with the red fluorescence from MTR (Fig. 2C). Pearson's correlation coefficient (Rr; from +1 to -1) was calculated to be 0.983, implying the high mitochondrion-targeting ability of **TPPCN**.

Another crucial parameter related to the resistance to photobleaching was also investigated using a confocal microscope under the continual scanning mode. As shown in Fig. 2E and F, the fluorescence of **TPPCN** could still be observed in mitochondria clearly and more than 95% of the signal was retained after 50 scans for about 13 min irradiation. In sharp contrast, over half of the fluorescence signal of MTR was lost after 25

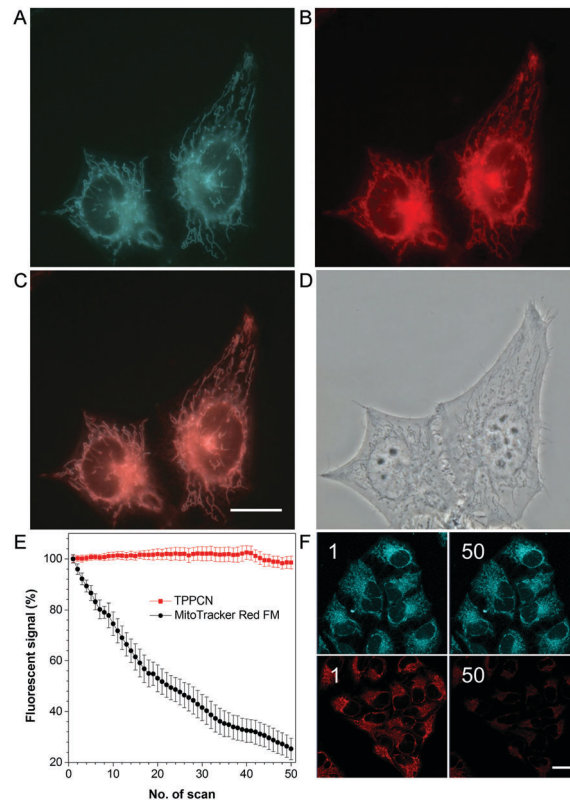


Fig. 2 (A and B) Fluorescence images of HeLa cells co-stained with (A) **TPPCN** (5 μM) and (B) MitoTracker red FM (MTR, 100 nM). (C) The merged images of (A) and (B). (D) Bright-field images of HeLa cells co-stained with **TPPCN** and MTR. Image conditions: λ_{ex} : 400–440 nm (**TPPCN**), 510–550 nm (MTR). (E) The plot of the fluorescent signal loss of HeLa cells co-stained with **TPPCN** (10 μM) and MTR (100 nM) against the increasing laser irradiation scans by using confocal laser scanning microscopy (CLSM). Conditions: λ_{ex} : 405 nm (**TPPCN**) and 560 nm (MTR); laser power: 6 μW (**TPPCN**), 2.16 μW (MTR). (F) CLSM images of HeLa cells co-stained with **TPPCN** (upper panel) and MTR (lower panel) before and after 50 laser irradiation scans (about 13 min). Scale bar: 20 μm .

scans and the red emission almost disappeared upon 50 scans. This clearly demonstrated that **TPPCN** possessed a higher photostability than MTR. Such superior photostability makes **TPPCN** capable for the long-term fluorescence imaging of cancer cells.

ROS production photosensitized by **TPPCN**

Inspired by the structural characteristic of the reported AIEgen-based photosensitizers,^{19e} the pyridinium and dicyanoethene units were envisioned to endow **TPPCN** with the ability of efficient ROS production. To this end, H2DCF-DA, a commonly-used ROS indicator, was utilized to confirm whether **TPPCN** can facilitate the generation of ROS upon light irradiation. H2DCF-DA could be specifically oxidized to generate a fluorescent emitter with high emission at around 530 nm in the presence of ROS.²⁵ Since **TPPCN** absorbed strongly in the region of visible light (Fig. 1B), white light from an incandescent lamp was utilized as the light source for ROS production. As shown in Fig. 3A, the fluorescence intensity of H2DCF-DA gradually enhanced with continuous light irradiation in the presence of **TPPCN**, while negligible fluorescence signal was detected for the irradiated solution

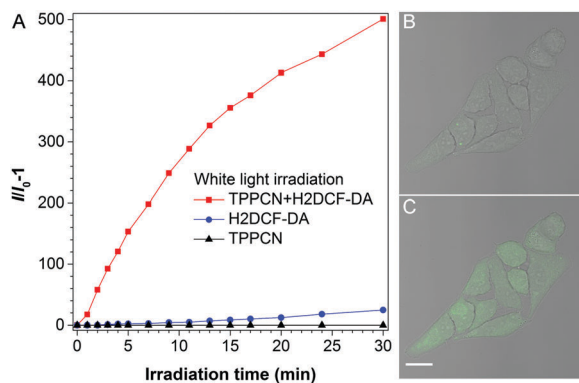


Fig. 3 Release of ROS monitored by H2DCF-DA. (A) Change in fluorescence intensity at 525 nm of **TPPCN** (10 μ M), H2DCF-DA (5 μ M), and their mixture in PBS solution upon white light irradiation for different time periods. Merged bright-field and fluorescence images of HeLa cells stained with **TPPCN** (10 μ M) for 10 min and H2DCF-DA (10 μ M) for 60 min before (B) and after (C) exposure to 405 nm laser for 10 s. λ_{ex} : 488 nm; scale bar: 20 μ m.

with **TPPCN** or H2DCF-DA alone. After illumination of white light for 30 min, the fluorescence intensity of H2DCF-DA was about 500 times higher than the initial intensity. In comparison to tetracycline, a commercially-available photosensitizer,²⁶ the rate of ROS production of **TPPCN** is much more efficient (see the ESI,† Fig. S12). Furthermore, Singlet Oxygen Sensor Green Reagent (SOSG) and HPF were also employed to check the type of ROS generated. SOSG is highly selective for Type 1 ROS (1O_2), while HPF is selective for highly reactive oxygen species (hROS) such as hydroxyl radical ($\bullet OH$), which belongs to Type 2 ROS.²⁷ As shown in Fig. S13A and B of the ESI,† the fluorescence intensity of HPF gradually enhanced with continuous light irradiation in the presence of **TPPCN** and reached about 400 times higher than the initial intensity after illumination of white light for 30 min. However, negligible fluorescence signal of SOSG was detected for the irradiated solution with **TPPCN** (see the ESI,† Fig. S13C). These results revealed that the **TPPCN** aggregates could generate Type 2 ROS in aqueous solution efficiently.

The ROS production of **TPPCN** inside cells was further investigated. Under a confocal laser scanning microscope, no fluorescence signal from H2DCF-DA could be detected in HeLa cells stained with **TPPCN** before 405 nm laser irradiation (Fig. 3B). Then, green emission from H2DCF-DA in HeLa cells was instantly observed upon 405 nm laser irradiation for only 10 s (Fig. 3C). However, the emission from the HeLa cells incubated with H2DCF-DA alone remained faint both before and after 405 nm laser irradiation (see the ESI,† Fig. S14). Consequently, **TPPCN** could trigger the ROS production inside cells under light irradiation. Owing to the detrimental effect of an excessive amount of ROS on cells, the mitochondria of **TPPCN**-stained HeLa cells changed from a long tubular-like morphology to small and dispersed fragments after irradiation for only 10 s, obviously indicative of the unhealthy state of HeLa cells induced by the ROS-mediated cell apoptosis.²⁸ By comparison, those treated without **TPPCN** still remained healthy under the same conditions (see the ESI,† Fig. S15).

Collectively, **TPPCN** could serve as a promising photosensitizer for PDT through the mitochondria-mediated cell apoptosis pathway.

Selective imaging and killing of cancer cells

Recent reports have demonstrated that positively charged AIEgens can distinguish cancer from normal cells intrinsically by taking advantage of the stronger electrostatic interactions between AIEgens and the mitochondria in cancer cells.²⁰ Hence, **TPPCN** with a positive charge was also endowed with the capability to differentiate cancer from normal cells. As shown in Fig. 4A, cancerous HeLa and normal MDCK-II cells were co-cultured in the same dish and then stained with **TPPCN**. Confocal images presented a strong blue-green fluorescence in the mitochondria of HeLa cells, while almost no fluorescence signal was detected in MDCK-II cells. This is due to the fact that the cancer cells have a higher MMP than normal cells,²⁹ which makes positively charged **TPPCN** more inclined to accumulate in the mitochondria of cancer cells and light up the cells (see the ESI,† Fig. S16 and S17).

According to the above discussion, we can conclude that **TPPCN** could not only act as a superior photosensitizer with high ROS production to induce cell apoptosis under white light irradiation but it could also especially light up the cancerous-type cells. Therefore, it has great potential for the selective imaging and killing of cancer cells over normal ones in the co-culture system. As shown in Fig. S18A of the ESI,† faint emission from H2DCF-DA was observed in the co-culture system containing both cancerous HeLa cells and normal MDCK-II ones before 405 nm laser irradiation. After 405 nm

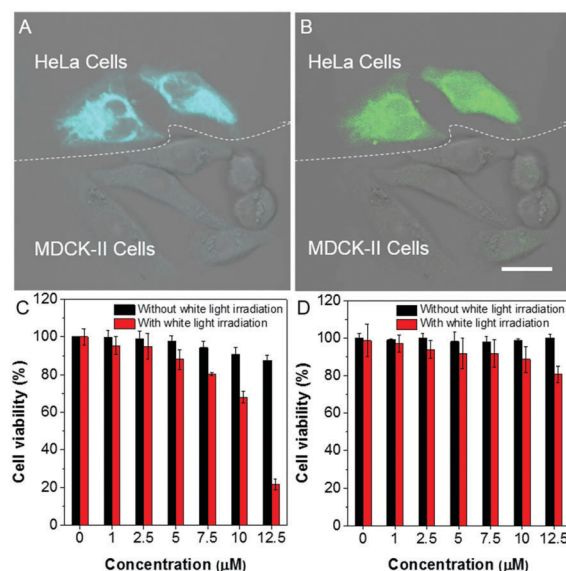


Fig. 4 Selective imaging and killing of cancer cells by **TPPCN**. (A and B) CLSM images of co-cultured HeLa and MDCK-II cells stained with **TPPCN** (10 μ M) and H2DCF-DA (10 μ M) (A) before and (B) after laser irradiation for 10 s (405 nm, 34 μ W). λ_{ex} : 405 nm (**TPPCN**), 488 nm (H2DCF-DA); scale bar: 20 μ m. (C and D) Cell viabilities of (C) HeLa cells and (D) MDCK-II cells in the presence of different concentrations of **TPPCN** with and without white light irradiation (36 mW).

laser irradiation for 10 s, the strong green emission from H2DCF-DA emerged only in HeLa cells, reflecting a large amount of ROS production, whereas only negligible emission was observed in MDCK-II cells (Fig. 4B). For the cells incubated with H2DCF-DA solely, negligible green emission was displayed both before and after 405 nm laser irradiation (see the ESI,† Fig. S18B and C). The results support that **TPPCN** can be photosensitized to generate efficient ROS only in cancer cells.

To further evaluate the PDT efficacy of **TPPCN** for cancer cells, MTT assays were applied to assess the cell viabilities of HeLa and MDCK-II cells. As shown in Fig. 4C and D, the cell viabilities for both HeLa and MDCK-II cells under white light irradiation were not affected in the absence of **TPPCN**. Upon incubation with **TPPCN**, the cell viability of HeLa cells decreased dramatically along with the increasing concentrations of **TPPCN** under white light illumination (Fig. 4C). In contrast, almost no obvious change in cell viability was observed for MDCK-II cells under the same conditions. More than 80% of HeLa cells were killed upon white light irradiation when the concentration of **TPPCN** was 12.5 μM , while the cell viability of MDCK-II cells still remained over 80% (Fig. 4D). It is worth noting that almost no change in cell viabilities was observed for both HeLa and MDCK-II cells when **TPPCN**-stained cells were kept in the dark. These results suggested that **TPPCN** could cause photodestruction to cancer cells over normal ones with the aid of light irradiation. Furthermore, propidium iodide (PI), which only stains dead or apoptotic cells with the late membrane damaged, was used to evaluate the therapeutic efficiency of **TPPCN** *via* PDT.³⁰ Only HeLa cells but not MDCK-II cells exhibited blue-green emission from **TPPCN** (see the ESI,† Fig. S19A). After white light irradiation, the red emission from PI was observed in all of the HeLa cells stained by **TPPCN**, indicating that these HeLa cells were effectively killed by the ROS generated by **TPPCN** (see the ESI,† Fig. S19). In sharp contrast, the blue-green emission cannot be observed in the MDCK-II cells, indicating that they cannot be stained by **TPPCN** (see the ESI,† Fig. S19E) and thus there is no ROS generation under treatment of white light. As a result, MDCK-II cells could not be stained by PI due to the impermeability of the membrane of the live cells (see the ESI,† Fig. S19). Besides, further experiments with other cell lines, including cancerous cells (U87, MCF7, PC3) and normal cells (LO2, 3T3), were also done to confirm the universal mitochondrion-specificity and cancer cell-selective killing of **TPPCN**. As shown in Fig. S20–S23 of the ESI,† **TPPCN** can target the mitochondria of cancer cells specifically and also act as an effective and selective photosensitizer for PDT of cancer cells. Collectively, **TPPCN** indeed could serve as an effective theranostic agent that would stain mitochondria specifically and induce death efficiently through PDT of cancer cells.

Selective imaging and killing of Gram-positive bacteria

Gram-negative bacteria possess more efficient barrier to the foreign substances than Gram-positive bacteria due to their more complicated envelope structure.²³ Therefore, it is envisioned that **TPPCN** is more inclined to enter the Gram-positive bacteria and then able to discriminate Gram-positive against Gram-negative bacteria.

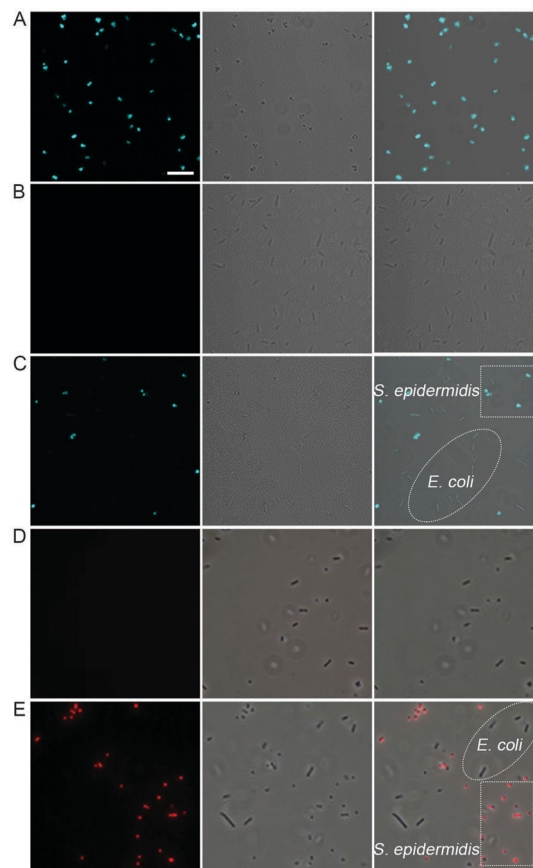


Fig. 5 (A–C) Selective imaging of Gram-positive bacteria. Fluorescence, bright-field and merged images of (A) *S. epidermidis*, (B) *E. coli* and (C) a mixture of them incubated with **TPPCN** for 10 min. Concentration: 10 μM ; λ_{ex} : 405 nm. (D and E) Effective killing of Gram-positive bacteria. Fluorescence, bright-field and merged images of the mixture of *S. epidermidis* and *E. coli* incubated (D) without and (E) with **TPPCN** (10 μM) for 10 min followed by white light exposure for 20 min, and then staining with PI (1.5 μM) for 15 min. λ_{ex} : 510–550 nm; scale bar: 10 μm .

To verify this hypothesis, two kinds of typical bacteria, Gram-positive *S. epidermidis* and Gram-negative *E. coli*, were selected as representatives for demonstration. As shown in Fig. 5A–C, *S. epidermidis* were stained and exhibited blue-green emission after incubation with **TPPCN** for 10 min. However, almost no emission was observed in *E. coli* as a result of the weaker staining capability of **TPPCN** towards Gram-negative bacteria. The co-culture system involving *S. epidermidis* and *E. coli* clearly demonstrated that *S. epidermidis* can be selectively distinguished from *E. coli* with intense blue-green emission. This result fully hinted that **TPPCN** has the potential to selectively discriminate Gram-positive from Gram-negative bacteria through fluorescence imaging techniques.

Besides the selective imaging ability for Gram-positive bacteria, **TPPCN** could be promisingly explored to selectively kill Gram-positive bacteria *via* PDT due to the outstanding role of the photosensitizer. A mixture of *S. epidermidis* and *E. coli* was incubated without or with **TPPCN** for 10 min, subsequently irradiated under white light for 20 min and then stained with PI. Both *S. epidermidis* and *E. coli* displayed almost no red

emission from PI when they were exposed to white light in the absence of TPPCN (Fig. 5D). However, the red fluorescence signal was clearly detected from *S. epidermidis* over *E. coli* in the presence of TPPCN (Fig. 5E). As PI selectively penetrates bacteria with damaged membranes displaying red emission,³⁰ it can be concluded that *S. epidermidis* were killed by the generated ROS of TPPCN, while *E. coli* were kept away from the killing effect of TPPCN, further supported by the results shown in Fig. S24 and S25 of the ESI.† Therefore, TPPCN could also be used to kill Gram-positive bacteria through PDT based on the ability of the photosensitizer.

To gain insights into the antibacterial effect of TPPCN on *S. epidermidis*, scanning electron microscopy (SEM) was used to test whether the bacterial death is ascribed to the destruction of the integrity of bacterial cell walls (see the ESI,† Fig. S25C and F). In the absence of TPPCN, the morphology of *S. epidermidis* remained regular, bearing the characteristics of clear borders and smooth bodies. The well-defined border between the overlapped bacteria was clearly resolved, indicative of the intact cell walls of *S. epidermidis*. Upon the treatment of TPPCN and white light irradiation, the cell walls of *S. epidermidis* shrunk and split, and the shape of bacteria also changed dramatically, definitely suggesting that the death of *S. epidermidis* was caused by the damage of their cell walls *via* PDT. Additionally, the plate-count method was also utilized to visually evaluate the antibacterial activity of TPPCN.³¹ The killing effect on *S. epidermidis* and *E. coli* by TPPCN-based PDT is shown in Fig. 6 through the photographs of solid agar plates. Without TPPCN, both *S. epidermidis* and *E. coli* grew healthy on the LB-agar plates. Light irradiation alone did not exert any obvious killing effect on the viability with the amount of *S. epidermidis* decreasing slightly (Fig. 6B). Almost no influence on the quantity of *E. coli* was exerted under both dark and light conditions (Fig. 6D and E). In the presence of both TPPCN and light irradiation, *S. epidermidis* were killed effectively and almost no colony formed on the plate (Fig. 6C), which implied the efficient PDT of TPPCN for *S. epidermidis*. The killing effect on *E. coli*, however, was negligible with the quantity of the colony unaffected (Fig. 6F).

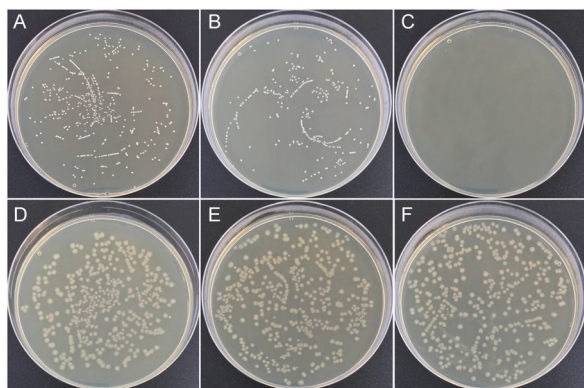


Fig. 6 Plates of *S. epidermidis* (A–C) and *E. coli* (D–F) without (A and D) and with (B and E) light irradiation for 30 min in the absence of TPPCN. Those treated with TPPCN (10 μ M) for 10 min, followed by irradiation with white light for 30 min are given in panels (C) and (F).

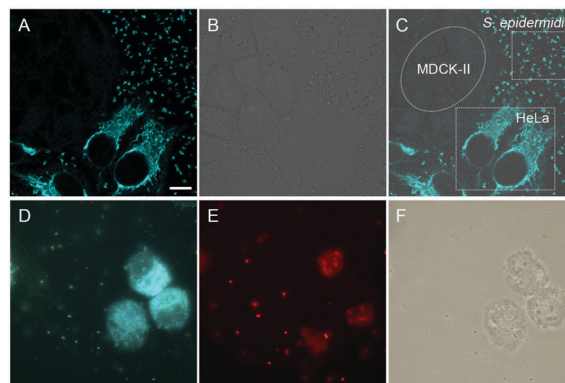


Fig. 7 (A–C) Selective imaging of *S. epidermidis* and HeLa cells. (A) Fluorescence, (B) bright-field and (C) merged images of a mixture of *S. epidermidis*, HeLa and MDCK-II cells incubated with TPPCN (10 μ M) for 10 min. λ_{ex} : 405 nm. (D–F) Effective killing of *S. epidermidis* and HeLa cells. Fluorescence images of a mixture of *S. epidermidis* and HeLa cells incubated with TPPCN (10 μ M) for 10 min (D), followed by staining with PI (1.5 μ M) for 15 min (E) after white light exposure for 60 min, and its respective bright-field images (F). λ_{ex} : 400–440 nm (TPPCN), 510–540 nm (PI); scale bar: 10 μ m.

Consequently, both SEM and plate-count method experiments are consistent with the conclusion that TPPCN could selectively kill Gram-positive over Gram-negative bacteria through the pathway of PDT.

Potential application of TPPCN in simultaneous imaging and killing of cancer cells and Gram-positive bacteria in a co-culture system

Finally, the capacity of TPPCN to simultaneously differentiate and kill both cancer cells and Gram-positive bacteria was further investigated in a multi-component system containing mammalian cells and bacteria (Fig. 7). Cancer cells (HeLa cells), normal cells (MDCK-II cells) and Gram-positive bacteria (*S. epidermidis*) were co-cultured in the same dish and stained with TPPCN. As shown in Fig. 7A–C, both HeLa cells and *S. epidermidis* were turned on selectively by TPPCN, while almost no fluorescence signal was detected from MDCK-II cells. Furthermore, after being illuminated by white light and subsequently incubating with PI, HeLa cells and *S. epidermidis* were clearly stained with red emission from PI, thus indicating the death of HeLa cells and *S. epidermidis* resulting from the mitochondrion-mediated cell apoptosis and the photoinduced bacterial cell wall destruction caused by ROS (Fig. 7D–F).^{28,30} This simple demonstration revealed that TPPCN is indeed a promising candidate for imaging and therapy applications in bacteria-associated cancer treatment involving the dual targeting function of cancer cells and Gram-positive bacteria.

Conclusions

In summary, an AIEgen, namely TPPCN, was simply designed and synthesized for the simultaneous imaging and killing of cancer cells and Gram-positive bacteria. TPPCN could selectively image cancer cells as well as Gram-positive bacteria with

the merits of superb sensitivity, good photostability, and a high signal-to-noise ratio. Meanwhile, **TPPCN** can generate ROS efficiently inside cancer cells and Gram-positive bacteria and cause oxidative damage to the mitochondria of cancer cells and cell walls of bacteria. This study not only validates the capability of AIEgens to differentiate cancer cells from normal ones, but also reasonably extends it to the identification of Gram-positive bacteria and Gram-negative ones. More significantly, it offers a general approach for constructing a multifunctional system that allows accurate cancer diagnosis and efficient therapy as well as associated-bacteria identification and killing. We expect that this work will motivate scientists to develop more novel AIEgens for comprehensive cancer treatments.

Experimental

Materials and instruments

Minimum essential medium (MEM), Dulbecco's modified Eagle medium (DMEM), fetal bovine serum (FBS), penicillin and streptomycin, phosphate buffered saline (PBS), Mito-Tracker Red FM, JC-1, Singlet Oxygen Sensor Green Reagent (SOSG), 3'-(*p*-hydroxyphenyl) fluorescein (HPF) and MitoSOX™ Red mitochondrial superoxide indicator were purchased from Invitrogen. LB agar and LB broth were purchased from USB Co. Propidium iodide (PI), H2DCF-DA, oligomycin A and carbonyl cyanide *m*-chlorophenyl hydrazine (CCCP) were purchased from Sigma-Aldrich. THF was purified by distillation from sodium benzophenone ketyl immediately prior to use. Other reagents used in this work, such as dimethyl sulfoxide, potassium chloride and sodium chloride, were purchased from Sigma-Aldrich and used as received without further purification. Milli-Q water was supplied by the Milli-Q Plus System (Millipore Corporation, United States). All the chemicals used in the synthesis of **TPPCN** were purchased from Sigma-Aldrich.

¹H and ¹³C NMR spectra were recorded on Bruker ARX 400 NMR spectrometers using CD₂Cl₂ as the deuterated solvent. High-resolution mass spectrometry (HRMS) was undertaken on a Finnegan MAT TSQ 7000 Mass Spectrometer System operating in a MALDI-TOF mode. The quantum yields were measured using a calibrated integrating sphere (Labsphere). UV absorption spectra were recorded on a Milton Ray Spectronic 3000 array spectrophotometer. Steady-state fluorescence spectra were recorded on a Perkin Elmer LS 55 spectrometer. Fluorescence images were collected on an Olympus BX 41 fluorescence microscope. Laser confocal scanning microscopy images were collected on a Zeiss laser scanning confocal microscope (LSM7 DUO) and analyzed using ZEN 2009 software (Carl Zeiss). The bacterial morphology was investigated using Scanning Electron Microscopy [JSM-6390 (JEOL)].

Synthesis and characterization of **TPPCN**

Synthesis of compound 1. Compound 1 was synthesized according to the literature.²⁴

Synthesis compound 2. TiCl₄ (1 mL, 9.0 mmol) was slowly added into a suspension of Zn dust (1.170 g, 18.0 mmol) in dry

THF (50 mL) at -78 °C. After refluxing for 2 h, a mixture of 4,4'-dimethoxyphenylmethanone (1.090 g, 4.5 mmol) and compound 1 (0.786 g, 3.0 mmol) in dry THF (20 mL) was added to the reaction. The mixture was continued to reflux for another 5 h. After removing the solvent using compressed air, the residue was extracted by DCM and dried over anhydrous Na₂SO₄. The crude product was purified on a silica-gel column using DCM as the eluent. Compound 2 was isolated as a yellow solid in 50% yield. ¹H NMR (400 MHz; CD₂Cl₂): δ = 8.33 (d, 2H), 7.31–7.28 (m, 2H), 6.96–6.91 (m, 8H), 6.71–6.69 (m, 2H), 3.77 ppm (d, 6H); ¹³C NMR (100 MHz; CD₂Cl₂): δ = 158.4, 158.2, 151.0, 148.7, 142.9, 141.5, 134.7, 134.4, 134.3, 132.4, 131.8, 131.7, 130.4, 125.3, 119.8, 112.6, 112.5, 54.5 ppm; HRMS (*m/z*) calcd for C₂₇H₂₂BrNO₂, [M]⁺: 471.0834; found, 471.0860.

Synthesis of compound 3. *n*-BuLi (0.6 mL, 1.2 mmol, 2.0 M in hexane) was added dropwise to a solution of compound 2 (0.471 g, 1.0 mmol) in dry THF (20 mL) at -78 °C under an atmosphere of N₂. After stirring for 2 h at this temperature, *N,N*-dimethylbenzamide (0.179 g, 1.2 mmol) was slowly added to the mixture and stirring was continued at -78 °C for 1 h. The mixture was then allowed to warm to room temperature (22 °C), quenched with 10% aqueous HCl (10 mL), and stirred for 30 min. The aqueous phase was separated and washed with DCM (3 × 10 mL), dried over anhydrous MgSO₄, and evaporated *in vacuo*. The crude product was subsequently reacted with malonitrile under refluxing with the assistance of TiCl₄ and pyridine, and the obtained mixture was purified on a silica gel column using DCM as the eluent to give compound 3 as a light-yellow solid (0.382 g, 70%). ¹H NMR (400 MHz; CD₂Cl₂): δ = 8.34 (d, 2H), 7.61–7.58 (m, 1H), 7.52–7.47 (m, 2H), 7.41–7.39 (m, 2H), 7.22 (d, 2H), 7.10 (d, 2H), 6.97–6.91 (m, 6H), 6.70 (d, 2H), 6.98 (d, 2H), 3.75 ppm (d, 6H); ¹³C NMR (100 MHz; CD₂Cl₂): δ = 174.2, 159.2, 159.1, 151.1, 149.5, 148.1, 145.2, 136.2, 135.1, 134.7, 134.6, 134.1, 132.6, 132.5, 132.4, 131.6, 130.4, 130.2, 128.7, 125.9, 114.1, 114.0, 113.3, 113.2, 81.1, 55.2 ppm; HRMS (*m/z*) calcd for C₃₇H₂₇N₃O₂, [M]⁺: 545.2103; found, 545.2369.

Synthesis of **TPPCN.** Briefly, a toluene solution of compound 3 (0.50 mmol) was added into CH₃I (5 mmol). The reaction mixture was heated and stirred under nitrogen at 110 °C for 4 h. The precipitate was collected and washed with toluene. The crude product was recrystallized using mixed solvents of hexane and dichloromethane. Then the pure product was dissolved in acetone and the counterion was exchanged with potassium hexafluorophosphate to obtain orange-color **TPPCN** with a yield of 90%. ¹H NMR (400 MHz; CD₂Cl₂): δ = 8.15 (d, 2H), 7.61 (t, 1H), 7.52 (t, 2H), 7.45–7.42 (m, 4H), 7.31 (d, 2H), 7.16 (d, 2H), 7.03 (d, 2H), 6.94 (d, 2H), 6.83 (d, 2H), 6.70 (d, 2H), 4.22 (s, 3H), 3.81 (s, 3H), 3.76 ppm (s, 3H); ¹³C NMR (100 MHz; CD₂Cl₂): δ = 174.0, 161.4, 161.0, 153.1, 146.0, 143.5, 135.8, 135.4, 133.3, 133.2, 132.7, 132.6, 132.0, 131.5, 130.9, 130.4, 129.7, 128.9, 114.4, 113.9, 113.8, 113.5, 81.7, 55.4, 55.3, 47.7 ppm; HRMS (*m/z*) calcd for C₃₈H₃₀N₃O₂⁺, [M]⁺: 560.2333, found: 560.2355.

Cell culture and cell imaging

HeLa cells were cultured in MEM. MDCK-II, MCF7, PC3, LO2, 3T3 and U87 cells were cultured in DMEM. For co-culture

experiments, the cells were cultured in DMEM. All the cells were cultured in media containing 10% FBS and antibiotics (100 units per mL penicillin and 100 g mL⁻¹ streptomycin) in a 5% CO₂ humidity incubator at 37 °C.

Cells were grown overnight on a 35 mm petri dish with a cover slip or a plasma-treated 25 mm round cover slip mounted at the bottom of a 35 mm petri dish with an observation window. The live cells were incubated with a certain dye at a certain concentration for a certain time (by adding 2 μL of a stock solution in DMSO solution to 2 mL of the cell culture medium, DMSO < 0.1 vol%). The dye-labelled cells were mounted and imaged under a fluorescence microscope (BX41 Microscope). Conditions: for **TPPCN**, excitation filter = 400–440 nm, dichroic mirror = 455 nm, and emission filter = 465 nm long pass; for MitoTracker red FM, excitation filter = 510–550 nm, dichroic mirror = 570 nm, and emission filter = 590 nm long pass. For the PI staining experiment, after 40 min incubation with 10 μM **TPPCN**, the cells were exposed to white light for 30 min (36 mW) and then incubated for 24 h in the dark, while the control group was placed in the dark throughout. Afterwards, PI was added to both the experiment and control groups at a final concentration of 1.5 μM, followed by incubation in the dark for another 15 min. Then, the cells were imaged under a fluorescence microscope with the following settings: excitation filter = 510–550 nm, dichroic mirror = 570 nm, and emission filter = 590 nm long pass. For the ROS generation experiments in cells, the cells were first incubated in a mixture of **TPPCN** (10 μM) and H₂DCF-DA (10 μM). All the images were then collected at different time periods of 405 nm laser irradiation using a 488 nm laser as excitation light. The spectral collection region was 500–550 nm.

Cytotoxicity studies

MTT assays were used to evaluate the cytotoxicity of **TPPCN** in the dark and under light irradiation. HeLa, MDCK-II or U87 cells were seeded in 96-well plates (Costar, IL, USA) at a density of 5×10^3 cells per well. After overnight culturing, the medium in each well was replaced by 100 μL of the fresh medium containing different concentrations of **TPPCN**. The volume fraction of DMSO is below 0.2%. For the biocompatibility test of **TPPCN** with HeLa cells, 24 hours later, 10 μL of MTT solution (5 mg mL⁻¹ in PBS) was added into each well. After 4 hours of incubation, 100 μL of SDS-HCl aqueous solution (10% SDS and 0.01 M HCl) was added to each well. After incubation for 6 hours, the absorption of each well at 595 nm was recorded using a plate reader (Perkin-Elmer Victor3™). For determining the cytotoxicity of **TPPCN** towards cancer cells and normal cells under light irradiation, after 8 h incubation, three plates containing HeLa, MDCK-II and U87 cells were exposed to white light (36 mW) for 30 min, and another three plates with cells were kept in the dark as control. Then, the cells were cultured for another 16 h in the incubator. Then, the plates were subjected to the same treatment as the biocompatibility test. Each trial was performed with 6 wells in parallel.

MMP quantification by JC-1

Cells were incubated with 2 μM JC-1 for 30 min and then the cells were imaged under a confocal microscope with the

following settings: green channel (λ_{ex} : 488 nm, λ_{em} : 515–545 nm) and red channel (λ_{ex} : 561 nm, λ_{em} : 575–590 nm). Other intensity data were measured using MATLAB R 2010b.

Photostability of TPPCN

The dye-labelled HeLa cells were imaged using a confocal microscope (Zeiss laser scanning confocal microscope LSM7 DUO) using ZEN 2009 software (Carl Zeiss). Conditions: for **TPPCN**, excitation wavelength: 405 nm; for MitoTracker red FM, excitation wavelength: 560 nm; laser powers were unified as 6 μW (**TPPCN**) and 2.16 μW (MTR).

Bacterial imaging

Prior to bacteria imaging, a single colony of bacteria on solid culture medium [Luria broth (LB) for *E. coli* and *S. epidermidis*] was transferred to 5 mL of the liquid culture medium and grown at 37 °C for 10 h. The concentrations of bacteria were determined by measuring the optical density at 600 nm (OD₆₀₀) and then 10⁹ colony forming unit (CFU) of bacteria was transferred to a 1.5 mL EP tube. Bacteria were harvested by centrifuging at 13 000 rpm for 3 min. After removal of the supernatant, 1 mL of the dye solution in PBS at a certain concentration was added into the EP tube. After dispersing with a vortex, the bacteria were incubated at room temperature for a certain time. To take fluorescence images, about 2 μL of the stained bacteria solution was transferred to a glass slide and then covered by a coverslip. The image was collected using a 100× objective. The bacteria were imaged under an FL microscope (BX41 Microscope) using the following settings: excitation filter = 400–440 nm, dichroic mirror = 455 nm, and emission filter = 465 nm long pass. For the PI staining experiment, after 10 min incubation with 10 μM **TPPCN**, the bacteria were exposed to white light for 20 min, while the control group was placed in the dark. Afterwards, PI was added to both the experiment and control groups at a final concentration of 1.5 μM, followed by incubation in the dark for another 15 min. Then, the bacteria were imaged under a fluorescent microscope with the following settings: excitation filter = 510–550 nm, dichroic mirror = 570 nm, and emission filter = 590 nm long pass.

Antimicrobial photodynamic inactivation

10⁸ CFU of bacteria was dispersed in 1 mL of PBS. After 10 min incubation with 10 μM **TPPCN**, the solution was centrifuged at 13 000 rpm for 3 min, followed by the removal of the supernatant and PBS washing. Then, the bacteria were dispersed in PBS and exposed to white light for designed periods of time, while the control groups were placed in the dark. Then, the viability of the bacteria was quantified by the plate-count method.

SEM studies

The concentration of *S. epidermidis* was diluted to an optical density of nearly 0.2 at 600 nm (OD₆₀₀). Then, they were incubated with 10 μM **TPPCN** for 4 h and illuminated with white light for 1 h, followed by drying, and collection of SEM images. Bacteria without treatment were also imaged under SEM for comparison.

Conflicts of interest

There are no conflicts of interest to declare.

Acknowledgements

This work was partially supported by the National Natural Science Foundation of China (NSFC) Grant (21788102, 81271476, 21702016), the Innovation and Technology Commission (ITC-CNERC14SC01) and the Research Grants Council of Hong Kong (16301614, 16305015, 16308016, N-HKUST604/14 and A-HKUST605/16). We also acknowledge the support from the Guangdong Innovative Research Team Program of China (201101C0105067115), the Science and Technology Plan of Shenzhen (JCYJ20160229205601482), the Guangzhou Science and Technology Research Grant (201300000154) and the 111 Project Grant (B13037).

Notes and references

- D. Hanahan and R. A. Weinberg, *Cell*, 2011, **144**, 646.
- (a) H. Lee, Y. Lee, C. Song, H. R. Cho, R. Ghaffari, T. Y. Choi, K. H. Kim, Y. B. Lee, D. Ling, H. Lee, S. J. Yu, S. H. Choi, T. Hyeon and D. H. Kim, *Nat. Commun.*, 2015, **6**, 10059; (b) H. Kuai, Z. Zhao, L. Mo, H. Liu, X. Hu, T. Fu, X. Zhang and W. Tan, *J. Am. Chem. Soc.*, 2017, **139**, 9128.
- (a) A. Llevot and D. Astruc, *Chem. Soc. Rev.*, 2012, **41**, 242; (b) M. J. Akhtar, M. Ahamed, H. A. Alhadlaq, S. A. Alrokayan and S. Kumar, *Clin. Chim. Acta*, 2014, **436**, 78; (c) L. Dai, J. Liu, Z. Luo, M. Li and K. Cai, *J. Mater. Chem. B*, 2016, **4**, 6758; (d) E. Pérez-Herrero and A. Fernández-Medarde, *Eur. J. Pharm. Biopharm.*, 2015, **93**, 52.
- B. D. Wallace, H. Wang, K. T. Lane, J. E. Scott, J. Orans, J. S. Koo, M. Venkatesh, C. Jobin, L. A. Yeh, S. Mani and M. R. Redinbo, *Science*, 2010, **330**, 831.
- (a) Y. Yang, W. Weng, J. Peng, L. Hong, L. Yang, Y. Toiyama, R. Gao, M. Liu, M. Yin, C. Pan, H. Li, B. Guo, Q. Zhu, Q. Wei, M. P. Moyer, P. Wang, S. Cai, A. Goel, H. Qin and Y. Ma, *Gastroenterology*, 2017, **152**, 851; (b) M. R. Rubinstein, X. Wang, W. Liu, Y. Hao, G. Cai and Y. W. Han, *Cell Host Microbe*, 2013, **14**, 195; (c) J. Abed, J. E. M. Emgård, G. Zamir, M. Faroja, G. Almogy, A. Grenov, A. Sol, R. Naor, E. Pikarsky, K. A. Atlan, A. Mellul, S. Chaushu, A. L. Manson, A. M. Earl, N. Ou, C. A. Brennan, W. S. Garrett and G. Bachrach, *Cell Host Microbe*, 2016, **20**, 215.
- L. T. Geller, M. Barzily-Rokni, T. Danino, O. H. Jonas, N. Shental, D. Nejman, N. Gavert, Y. Zwang, Z. A. Cooper, K. Shee, C. A. Thaiss, A. Reuben, J. Livny, R. Avraham, D. T. Frederick, M. Ligorio, K. Chatman, S. E. Johnston, C. M. Mosher, A. Brandis, G. Fuks, C. Gurbatri, V. Gopalakrishnan, M. Kim, M. W. Hurd, M. Katz, J. Fleming, A. Maitra, D. A. Smith, M. Skalak, J. Bu, M. Michaud, S. A. Trauger, I. Barshack, T. Golan, J. Sandbank, K. T. Flaherty, A. Mandinova, W. S. Garrett, S. P. Thayer, C. R. Ferrone, C. Huttenhower, S. N. Bhatia, D. Gevers, J. A. Wargo, T. R. Golub and R. Straussman, *Science*, 2017, **357**, 1156.
- T. Yu, F. Guo, Y. Yu, T. Sun, D. Ma, J. Han, Y. Qian, I. Kryczek, D. Sun, N. Nagarsheth, Y. Chen, H. Chen, J. Hong, W. Zou and J. Y. Fang, *Cell*, 2017, **170**, 548.
- S. Bullman, C. S. Pedamallu, E. Sicinska, T. E. Clancy, X. Zhang, D. Cai, D. Neuberg, K. Huang, F. Guevara, T. Nelson, O. Chipashvili, T. Hagan, M. Walker, A. Ramachandran, B. Diosdado, G. Serna, N. Mulet, S. Landolfi, S. R. Cajal, R. Fasani, A. J. Aguirre, K. Ng, E. Élez, S. Ogino, J. Tabernero, C. S. Fuchs, W. C. Hahn, P. Nuciforo and M. Meyerson, *Science*, 2017, **358**, 1443.
- (a) N. M. Bagnall, S. Vig and P. Trivedi, *Surgery*, 2009, **27**, 426; (b) D. J. Leaper, *Br. J. Surg.*, 2010, **97**, 1601.
- (a) S. S. Kelkar and T. M. Reineke, *Bioconjugate Chem.*, 2011, **22**, 1879; (b) G. Feng and B. Liu, *Small*, 2016, **12**, 6528; (c) J. M. Idée, S. Louguet, S. Ballet and C. Corot, *Quant. Imaging Med. Surg.*, 2013, **3**, 292; (d) N. H. Cho, T. C. Cheong, J. H. Min, J. H. Wu, S. J. Lee, D. Kim, J. S. Yang, S. Kim, Y. K. Kim and S. Y. Seong, *Nat. Nanotechnol.*, 2011, **6**, 675.
- C. Chi, Y. Du, J. Ye, D. Kou, J. Qiu, J. Wang, J. Tian and X. Chen, *Theranostics*, 2014, **4**, 1072.
- (a) B. S. Reisner and G. L. Woods, *J. Clin. Microbiol.*, 1999, **37**, 2024; (b) M. P. Weinstein, S. Mirrett, L. G. Reimer, M. L. Wilson, S. Smith-Elekes, C. R. Chuard, K. L. Joho and L. B. Reller, *J. Clin. Microbiol.*, 1995, **33**, 978; (c) J. Wang, X. Wang, Y. Li, S. Yan, Q. Zhou, B. Gao, J. Peng, J. Du, Q. Fu, S. Jia, J. Zhang and L. Zhan, *Anal. Sci.*, 2012, **28**, 237; (d) Y. Hu, J. Liu, D. Xia and S. Chen, *J. Basic Microbiol.*, 2012, **52**, 27; (e) U. Ruffing, R. Akulenko, M. Bischoff, V. Helms, M. Herrmann and L. Müller, *PLoS One*, 2012, **7**, e52487.
- (a) A. L. Vahrmeijer, M. Hutteman, J. R. van der Vorst, C. J. H. van de Velde and J. V. Frangioni, *Nat. Rev. Clin. Oncol.*, 2013, **10**, 507; (b) J. Kim, Y. Piao and T. Hyeon, *Chem. Soc. Rev.*, 2009, **38**, 372; (c) R. Bardhan, S. Lal, A. Joshi and N. J. Halas, *Acc. Chem. Res.*, 2011, **44**, 936.
- (a) S. M. Borisov and O. S. Wolfbeis, *Chem. Rev.*, 2008, **108**, 423; (b) M. Nuriya, S. Fukushima, A. Momotake, T. Shinotsuka, M. Yasui and T. Arai, *Nat. Commun.*, 2016, **7**, 11557; (c) X. C. Zheng, X. Wang, H. Mao, W. Wu, B. R. Liu and X. Q. Jiang, *Nat. Commun.*, 2015, **6**, 5834; (d) W. Chen, Q. Li, W. Zheng, F. Hu, G. Zhang, Z. Wang, D. Zhang and X. Jiang, *Angew. Chem.*, 2014, **126**, 13954.
- T. Förster and K. Kasper, *Z. Phys. Chem.*, 1954, **1**, 275.
- (a) U. Resch-Genger, M. Grabolle, S. Cavaliere-Jaricot, R. Nitschke and T. Nann, *Nat. Methods*, 2008, **5**, 763; (b) A. M. Derfus, W. C. W. Chan and S. N. Bhatia, *Nano Lett.*, 2004, **4**, 11.
- (a) J. Luo, Z. Xie, J. W. Y. Lam., Y. Dong, S. M. F. Lo, I. D. Williams, D. Zhu and B. Z. Tang, *Chem. Commun.*, 2001, 1740; (b) B. Liu, A. Pucci and T. Baumgartner, *Mater. Chem. Front.*, 2017, **1**, 1689.
- (a) J. Mei, N. L. C. Leung, R. T. K. Kwok, J. W. Y. Lam and B. Z. Tang, *Chem. Rev.*, 2015, **115**, 11718; (b) R. T. K. Kwok, C. W. T. Leung, J. W. Y. Lam and B. Z. Tang, *Chem. Soc. Rev.*, 2015, **44**, 4228; (c) M. Kang, X. Gu, R. T. K. Kwok, C. W. T. Leung, J. W. Y. Lam, F. Li and B. Z. Tang, *Chem. Commun.*,

- 2016, **52**, 5957; (d) X. Gu, E. Zhao, T. Zhao, M. Kang, C. Gui, J. W. Y. Lam, S. Du, M. M. T. Loy and B. Z. Tang, *Adv. Mater.*, 2016, **28**, 5064; (e) X. Shi, C. Y. Y. Yu, H. Su, R. T. K. Kwok, M. Jiang, Z. He, J. W. Y. Lam and B. Z. Tang, *Chem. Sci.*, 2017, **8**, 7014; (f) M. Jiang, X. Gu, J. W. Y. Lam, Y. Zhang, R. T. K. Kwok, K. S. Wong and B. Z. Tang, *Chem. Sci.*, 2017, **8**, 5440.
- 19 (a) M. Gao, Q. Hu, G. Feng, N. Tomczak, R. Liu, B. Xing, B. Z. Tang and B. Liu, *Adv. Healthcare Mater.*, 2015, **4**, 659; (b) Y. Yuan, C. J. Zhang, M. Gao, R. Zhang, B. Z. Tang and B. Liu, *Angew. Chem., Int. Ed.*, 2015, **54**, 1780; (c) G. Feng, Y. Fang, J. Liu, J. Geng, D. Ding and B. Liu, *Small*, 2017, **13**, 1602807; (d) J. Qian and B. Z. Tang, *Chem*, 2017, **3**, 56; (e) X. Gu, R. T. K. Kwok, J. W. Y. Lam and B. Z. Tang, *Biomaterials*, 2017, **146**, 115; (f) N. Alifu, X. Dong, D. Li, X. Sun, A. Zebibula, D. Zhang, G. Zhang and J. Qian, *Mater. Chem. Front.*, 2017, **1**, 1746.
- 20 (a) C. Gui, E. Zhao, R. T. K. Kwok, A. C. S. Leung, J. W. Y. Lam, M. Jiang, H. Deng, Y. Cai, W. Zhang, H. Su and B. Z. Tang, *Chem. Sci.*, 2017, **8**, 1822; (b) L. B. Chen, *Annu. Rev. Cell Biol.*, 1988, **4**, 155.
- 21 (a) M. Jiang, X. Gu, R. T. K. Kwok, Y. Li, H. H. Y. Sung, X. Zheng, Y. Zhang, J. W. Y. Lam, I. D. Williams, X. Huang, K. S. Wong and B. Z. Tang, *Adv. Funct. Mater.*, 2018, **28**, 1704589; (b) E. Zhao, Y. Chen, S. Chen, H. Deng, C. Gui, C. W. T. Leung, Y. Hong, J. W. Y. Lam and B. Z. Tang, *Adv. Mater.*, 2015, **27**, 4931; (c) E. Zhao, Y. Hong, S. Chen, C. W. T. Leung, C. Y. K. Chan, R. T. K. Kwok, J. W. Y. Lam and B. Z. Tang, *Adv. Healthcare Mater.*, 2014, **3**, 88; (d) C. Zhu, Q. Yang, L. Liu, F. Lv, S. Li, G. Yang and S. Wang, *Adv. Mater.*, 2011, **23**, 4805; (e) C. Zhu, Q. Yang, L. Liu and S. Wang, *Angew. Chem., Int. Ed.*, 2011, **50**, 9607.
- 22 (a) G. Feng, Y. Yuan, H. Fang, R. Zhang, B. Xing, G. Zhang, D. Zhang and B. Liu, *Chem. Commun.*, 2015, **51**, 12490; (b) X. Zhang, X. Chen, J. Yang, H. R. Jia, Y. H. Li, Z. Chen and F. G. Wu, *Adv. Funct. Mater.*, 2016, **26**, 5958.
- 23 (a) H. X. Yuan, Z. Liu, L. B. Liu, F. Lv, Y. L. Wang and S. Wang, *Adv. Mater.*, 2014, **26**, 4333; (b) Y. Wang, T. S. Corbitt, S. D. Jett, Y. Tang, K. S. Schanze, E. Y. Chi and D. G. Whitten, *Langmuir*, 2012, **28**, 65; (c) G. McDonnell and A. D. Russell, *Clin. Microbiol. Rev.*, 1999, **12**, 147.
- 24 X. Tao, W. Li, X. Ma, X. Li, W. Fan, X. Xie, T. Ayad, V. Ratovelomanana-Vidal and Z. Zhang, *J. Org. Chem.*, 2012, **77**, 612.
- 25 M. Karbowski and R. J. Youle, *Cell Death Differ.*, 2003, **10**, 870.
- 26 J. A. Wiebe and D. E. Moore, *J. Pharm. Sci.*, 1977, **66**, 186.
- 27 (a) C. Rota, C. F. Chignell and R. P. Mason, *Free Radical Biol. Med.*, 1999, **27**, 873; (b) K. Setsukinai, Y. Urano, K. Kakinuma, H. J. Majima and T. Nagano, *J. Biol. Chem.*, 2003, **278**, 3170.
- 28 D. F. Suen, K. L. Norris and R. J. Youle, *Genes Dev.*, 2008, **22**, 1577.
- 29 B. C. Lan, *Annu. Rev. Cell Biol.*, 1988, **4**, 155.
- 30 L. Boullos, M. Prevost, B. Barbeau, J. Coallier and R. Desjardins, *J. Microbiol. Methods*, 1999, **37**, 77.
- 31 (a) A. S. Kaprelyants and D. B. Kell, *J. Appl. Bacteriol.*, 1992, **72**, 410; (b) P. Breeuwer and T. Abee, *Int. J. Food Microbiol.*, 2000, **55**, 193.